Available online at www.sciencedirect.com
ScienceDirect
Journal of Sound and Vibration 301 (2007) 521–543
JOURNAL OF SOUND AND VIBRATION
www.elsevier.com/locate/jsvi

Optimal placement and active vibration control for piezoelectric smart flexible cantilever plate

Zhi-cheng Qiu[a,*], Xian-min Zhang[a], Hong-xin Wu[b], Hong-hua Zhang[b]

[a]*School of Mechanical Engineering, South China University of Technology, Guangzhou 510641, PR China*
[b]*Beijing Institute of Control Engineering, Chinese Academy of Space Technology, Beijing 100080, PR China*

Received 4 September 2005; received in revised form 29 August 2006; accepted 9 October 2006
Available online 4 December 2006

Abstract

Some flexible appendages of spacecraft are cantilever plate structures, such as sun plate and satellite antenna. Thus, vibration problem will be caused by parameter uncertainties and environmental disturbances. In this paper, piezoelectric ceramics patches are used as sensors and actuators to suppress the vibration of the smart flexible clamped plate. Firstly, modal equations and piezoelectric control equations of cantilever plate are derived. Secondly, an optimal placement method for the locations of piezoelectric actuators and sensors is developed based on the degree of observability and controllability indices for cantilever plate. The bending and torsional modes are decoupled by the proposed method using bandwidth Butterworth filter. Thirdly, an efficient control method by combining positive position feedback and proportional-derivative control is proposed for vibration reduction. The analytical results for modal frequencies, transient responses and control responses are carried out. Finally, an experimental setup of piezoelectric smart plate is designed and built up. The modal frequencies and damping ratios of the plate setup are obtained by identification method. Also, the experimental studies on vibration control of the cantilever plate including bending modes and torsional modes are conducted. The analytical and experimental results demonstrate that the presented control method is feasible, and the optimal placement method is effective.

1. Introduction

With the development of the space technology, space structures are becoming larger and more flexible, whose modal frequencies and damping ratios are relatively low. In order to meet the high precision requirement of large space structures, the application of active control for vibration suppression becomes more and more important than ever before [1]. In recent years, smart materials, such as piezoelectric transducers, have been used extensively as distributed sensors and actuators for vibration control of flexible structures [2].

Smart structures have been attracted significant attention in the field of control and dynamics, and many achievements have been made in the past ten years. For one-dimension analysis of beam, we shall follow the

*Corresponding author. Tel.: +86 20 8711 4635; fax: +86 20 8711 3431.
E-mail addresses: zhchqiu@scut.edu.cn, zhchqiu@126.com (Z.-c. Qiu).

0022-460X/$ - see front matter © 2006 Elsevier Ltd. All rights reserved.
doi:10.1016/j.jsv.2006.10.018

early work of Bailey and Hubbard [3], Crawley and Luis [4]. In 1985, Bailey and Hubbard [3] developed first adaptive structure using polyvinylidene fluoride (PVDF) film as the distributed actuator to perform structural vibration control of cantilever beam. Since then, analytical models for the smart beams, plates, and shells integrated with the piezoelectric actuators and sensors have been established. Crawley et al. [4,5] discussed on the modeling technique applicable to the beam structure bonded with piezoceramic (PZT) sensors and actuators. Tzou and Fu [6], Fuller et al. [7], Clark et al. [8] developed a dynamics model for the vibration response of a simply supported elastic rectangular plate using a piezoelectric patch of variable rectangular geometry. In the case of flexible structures, the projection of physical displacements on a modal basis allows the observation and the control of each mode by independent sensors and actuators. However, projection in modal space, then modal reduction in the observation and control bands, leads to a risk of instability of the non-controlled modes: spillover [10]. Therefore, in implementing the control of flexible structures, the problem of spillover must be considered.

Many control algorithms were used to suppress the vibration, such as direct velocity feedback (DVFB) control, acceleration feedback control and positive position feedback (PPF) control [12], etc. Independent modal space control (IMSC) [9] is an effective method for vibration control of smart structures, in which the collocated modal sensor and modal actuator are needed. Lee and Moon [11] have considered the design of two-dimensional modal sensors. In their studies, it is more difficult to shape the sensor to obtain the necessary sensor weighting since variation in the vibration profile occurs in both x and y directions. Bailey and Hubbard [3] used induced strain actuation as part of output feedback, applied velocity feedback control algorithms to suppress the vibration of cantilever beam. Fanson and Caughy [12] proposed the PPF control method based on the modal displacement signal. The PPF controller is very effective in suppressing the specific vibration mode, thus, maximizing the damping in target frequency band without destabilizing other mode. Shimon et al. [13] studied a fully clamped plate problem theoretically and experimentally. In their studies, inertial actuators or distributed strain actuators were utilized, and positive velocity feedback (PVF) and H_∞ control methods were adopted to suppress the first mode vibration of the plate.

Structure vibration suppression depends not only on control law design but also on sensors/actuators selection and placement [14]. Sensors and actuators used in active control of smart structures have to be located appropriately to ensure maximum control and measurement effectiveness. The locations of sensors and actuators for an open-loop system influence the controllability and observability properties of the system. One must modify the locations of sensors and actuators to obtain the required values of the controllability and observability grammians. Thus, the placement of actuators and sensors is very important for effective control of structure using smart materials. The methods for optimal placement of sensors s and actuator were investigated by many researchers [14–18]. A typical solution to the location problem is found through a search procedure. For large numbers of locations, the search for the number of possible combinations is overwhelming and only a small selected subset is searched. This is time consuming and not necessarily the optimal solution [15]. So, it is vital to find an optimal placement method for piezoelectric smart plate.

In this paper, active vibration control of smart flexible cantilever plate is investigated by using discrete piezoelectric sensors and actuators. Optimal placement of sensors and actuators is processed based on piezoelectric control equation. To suppress the first three vibration modes of the cantilever plate, including bending modes and torsional mode, a controller by combining PPF and proportional-derivative (PD) is presented. Both theoretical and experimental studies are carried out to verify the advantage of the presented method.

The rest of the article is organized as follows: The modal equations and the piezoelectric control equations with distributed piezoelectric actuators for cantilever plate including bending and torsional modes are obtained in Section 2. In Section 3, the optimal placement method of piezoelectric sensors and actuators for cantilever plate is given according to maximum observability and controllability rule by using H_2 norm. In Section 4, the control algorithm by combining PPF and PD is proposed, and its stability and advantages are theoretically analyzed. The numerical simulations are carried out with different control methods. In Section 5, an experimental setup of piezoelectric smart plate for active vibration control is designed and built up. The modal frequencies and damping ratios of the plate system are identified experimentally. Based on these parameters, the proposed control method for the first three vibration modes is designed to control the system. Finally, the conclusions are given in Section 6.

2. Basic equations

2.1. Modal equations of cantilever plate

Based on the hypothesis of Kirchhoff–Love, the free vibration equation of the two-dimensional rectangular plate is [7]

$$D_p\left(\frac{\partial^4}{\partial x^4}+2\frac{\partial^4}{\partial x^2\partial y^2}+\frac{\partial^4}{\partial y^4}\right)w(x,y,t)+\rho_p h\frac{\partial^2 w(x,y,t)}{\partial t^2}=0, \tag{1}$$

where $w(x,y,t)$ is the transverse modal displacement, $D_p=E_p h^3/12\left(1-v_p^2\right)$ is flexural rigidity, E_p is Young's modulus, v_p is Poisson's ratio, h is the thickness of the plate, ρ_p is the density of plate material, x and y are the coordinate variables of the plate, and t is time variable.

According to Ritz's method, the total transverse displacement $w(x,y,t)$ at any point on the plate can be expressed as a time-dependent weighted sum of assumed spatial mode shape functions

$$w(x,y,t)=\sum_{m=1}^{\infty}\sum_{n=1}^{\infty}W_{mn}(x,y)\eta_{mn}(t), \tag{2}$$

where the subscripts m and n denote the (m, n)th mode of vibration, $W_{mn}(x,y)$ denote the modal function of the plate, $\eta_{mn}(t)$ denote the modal coordinate.

Because the analytical solution of the cantilever plate modes cannot be obtained directly, the modal trial function method is used to express the modal functions approximately. These Ritz functions $W_{mn}(x,y)$ are products of modal functions corresponding to the two beams associated with the boundary conditions of the plate. For cantilever plate, $W_{mn}(x,y)$ are in turn products of assumed free-free beam modes, $Y_n(y)$, in the chordwise direction and clamped-free beam modes, $X_m(x)$, in the spanwise direction. They are expressed as following [19]

$$W_{mn}(x,y)=X_m(x)\,Y_n(y), \tag{3}$$

where

$$X_m(x)=\cosh(k_m x)-\cos(k_m x)-\frac{\sinh(k_m l)-\sin(k_m l)}{\cosh(k_m l)+\cos(k_m l)}\times[\sinh(k_m x)-\sin(k_m x)],\quad m=1,2,3,\ldots, \tag{4}$$

$$Y_n(y)=\begin{cases}1, & n=1,\\ \sqrt{3}\left(1-\dfrac{2y}{l}\right), & n=2,\\ \sin(k_n y)+\sinh(k_n y)+\dfrac{\cos(k_n l)-\cosh(k_n l)}{\sin(k_n l)+\sinh(k_n l)}[\cos(k_n y)+\cosh(k_n y)], & n\geqslant 3.\end{cases} \tag{5}$$

The potential energy U and kinetic energy T of the plate can be expressed as

$$U=\frac{1}{2}D_p\iint\left[\left(\frac{\partial^2 w}{\partial x^2}+\frac{\partial^2 w}{\partial y^2}\right)^2-2(1-v_p)\left\{\frac{\partial^2 w}{\partial x^2}\frac{\partial^2 w}{\partial y^2}-\left(\frac{\partial^2 w}{\partial x\partial y}\right)^2\right\}\right]\mathrm{d}x\mathrm{d}y=\frac{1}{2}q^{\mathrm{T}}K_p q, \tag{6}$$

$$T=\frac{1}{2}\rho_p h\iint\left(\frac{\partial w}{\partial t}\right)^2\mathrm{d}x\mathrm{d}y=\frac{1}{2}\dot{q}^{\mathrm{T}}M_p\dot{q}, \tag{7}$$

where M_p and K_p are the stiffness matrix and mass matrix of the plate, respectively; the dots denote the derivatives with respect to time t; q is the modal coordinate vector, and it is

$$q=\left[\eta_{11}\ \eta_{21}\ \eta_{12}\ldots\eta_{mn}\right]^{\mathrm{T}}.$$

Substituting the modal trial function (3) into Eqs. (6) and (7), the stiffness matrix and the mass matrix of the plate can be derived. For simplification, let $\Phi_i = W_{pq}(x,y) = X_p(x)Y_q(y)$, and based on Eq. (2) and Refs. [8,25], the ith row and the jth column elements of the stiffness matrix and mass matrix for the plate can be computed using Eqs. (8) and (9), respectively

$$K_{pij} = \frac{E_p h^3}{12\left(1-v_p^2\right)} \int_0^a \int_0^b \left[\frac{\partial^2 \Phi_i}{\partial x^2}\frac{\partial^2 \Phi_j}{\partial x^2} + \frac{\partial^2 \Phi_i}{\partial y^2}\frac{\partial^2 \Phi_j}{\partial y^2} + v_p\left(\frac{\partial^2 \Phi_i}{\partial x^2}\frac{\partial^2 \Phi_j}{\partial y^2} + \frac{\partial^2 \Phi_i}{\partial y^2}\frac{\partial^2 \Phi_j}{\partial x^2}\right) + 2\left(1-v_p\right)\frac{\partial^2 \Phi_i}{\partial x \partial y}\frac{\partial^2 \Phi_j}{\partial x \partial y}\right] \mathrm{d}x\mathrm{d}y, \tag{8}$$

$$M_{pij} = \rho_p h \int_0^a \int_0^b \Phi_i(x,y)\Phi_j(x,y)\,\mathrm{d}x\mathrm{d}y. \tag{9}$$

By using modal analysis method, the stiffness matrix and the mass matrix can be expressed as

$$K_p = D_p\left\{X^{(22)} \otimes Y^{(00)} + X^{(00)} \otimes Y^{(22)} + v_p\left(X^{(20)} \otimes Y^{(02)} + X^{(02)} \otimes Y^{(20)}\right) + 2\left(1-v_p\right)\left(X^{(11)} \otimes Y^{(11)}\right)\right\}, \tag{10}$$

$$M_p = \rho_p h\left(X^{(00)} \otimes Y^{(00)}\right), \tag{11}$$

where sign $\otimes$ indicates Kronecker product; and

$$X_{ij}^{(22)} = \int_0^a X_i'' X_j''\,\mathrm{d}x, \quad X_{ij}^{(20)} = \int_0^a X_i'' X_j\,\mathrm{d}x,$$
$$X_{ij}^{(02)} = \int_0^a X_i X_j''\,\mathrm{d}x, \quad X_{ij}^{(00)} = \int_0^a X_i X_j'\,\mathrm{d}x, \quad X_{ij}^{(11)} = \int_0^a X_i' X_j\,\mathrm{d}x,$$
$$Y_{ij}^{(22)} = \int_0^b Y_i'' Y_j''\,\mathrm{d}y, \quad Y_{ij}^{(20)} = \int_0^b Y_i'' Y_j\,\mathrm{d}y,$$
$$Y_{ij}^{(02)} = \int_0^b Y_i Y_j''\,\mathrm{d}y, \quad Y_{ij}^{(11)} = \int_0^b Y_i' Y_j'\,\mathrm{d}y, \quad Y_{ij}^{(00)} = \int_0^b Y_i Y_j\,\mathrm{d}y,$$

where the primes denote the derivatives with respect to space variable x.

According to the Rayleigh–Ritz's method, the kth natural modal frequency ω_k of the plate is given as

$$\omega_k = \sqrt{\lambda_k\left(\left[M_p\right]^{-1}\left[K_p\right]\right)}, \tag{12}$$

where $\lambda_k(\cdot)$ is the kth eigenvalue.

When the structural size and material parameters of the plate are known, the natural modal frequencies can be calculated by solving Eq. (12). The calculated results are helpful to process the problem of the optimal placement of sensors and actuators, and can be used in analytical study of active control algorithms for plate system.

2.2. Piezoelectric control equations of the plate

In the experimental system, the piezoelectric sensors and actuators are bonded to the flexible structure using strong adhesive material. The schematic diagram of cantilever plate with bonded rectangular actuators is shown in Fig. 1. When the orientation angle $\beta \neq 0$, both the bending modes and torsional modes can be measured and controlled. When $\beta = 0$, only the bending modes can be measured and controlled.

The electric current generated by the ith sensor element can be written as [8]

$$I_i(t) = -r_i \int\int_{S_{ni}} \left(e_{31i}\frac{\partial^3 w}{\partial x^2 \partial t} + e_{32i}\frac{\partial^3 w}{\partial y^2 \partial t} + 2e_{36i}\frac{\partial^3 w}{\partial x \partial y \partial t}\right) \mathrm{d}x\mathrm{d}y, \quad i = 1,2,\ldots,N_s, \tag{13}$$

where $S_{ni}(x_{1n} \leqslant x \leqslant x_{2n}\ y_{1n} \leqslant y \leqslant y_{2n})$ denotes the area of the ith piezoelectric sensor element; e_{31i} and e_{36i} denote piezoelectric stress constants of the ith piezoelectric sensor; r_i denotes the distance between the middle plane of the ith sensor and that of the plate.

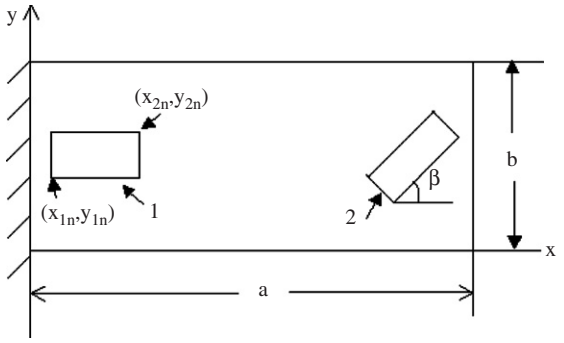

Fig. 1. The schematic diagram of the piezoelectric smart cantilever plate.

From Eq. (13), the sensor's output coefficients can be expressed as

$$\text{sensor}_{mn}^{i} = -r_i \int\int_{S_{ni}} \left(e_{31i} \frac{\partial^2 W_{mn}(x,y)}{\partial x^2} + e_{32i} \frac{\partial^2 W_{mn}(x,y)}{\partial y^2} + 2e_{36i} \frac{\partial^2 W_{mn}(x,y)}{\partial x \partial y} \right) \mathrm{d}x\mathrm{d}y. \tag{14}$$

The magnitude of the induced strains can be expressed as

$$\varepsilon_{pe}^{n} = \frac{d_{31n}}{h_{an}} V_n, \tag{15a}$$

$$\varepsilon_{pe6}^{n} = \frac{d_{36n}}{h_{an}} V_n, \tag{15b}$$

where ε_{pe}^{n} and ε_{pe6}^{n} are the resultant strains of the nth piezoelectric actuator; d_{31n} and d_{36n} are the piezoelectric material strain constants; V_n is the applied voltage in the direction of polarization; h_{an} is the thickness of the piezoelectric actuator.

The piezoelectric actuators will induce internal moments in both the x and y directions, which are only present under the condition that the piezoelectric patch extends. These bending moments, m_x and m_y, induced by the actuators can be written as [7]

$$m_x = m_y = C_0^n \varepsilon_{pe} [H(x - x_1) - H(x - x_2)] \left[H\left(y - y_1\right) - H\left(y - y_2\right) \right], \tag{16}$$

where $H(\cdot)$ is unit Heaviside (step) function; C_0^n is the coefficient of the piezoelectric plate for the nth piezoelectric patch, and it can be written as [7]

$$C_0^n = -\frac{2}{3} \frac{1 + v_{\text{pen}}}{1 - v_p} \frac{E_p h_p^2 P_n}{1 + v_p - \left(1 + v_{\text{pen}}\right) P_n}, \tag{17}$$

$$P_n = -\frac{E_{\text{pen}}}{E_p} \frac{1 - v_p^2}{1 - v_{\text{pen}}^2} \frac{3 h_{an} h_p \left(2h_p + h_{an}\right)}{2\left(h_p^3 + h_{an}^3\right) + 3h_p h_{an}^2}, \tag{18}$$

where E_{pen} and v_{pen} are Young's modulus, Poisson's ratio of the piezoelectric actuator, respectively; h_p is the half thickness of the plate.

Similarly, the induced torsional moment m_{xy} can be expressed as

$$m_{xy} = C_0^n \varepsilon_{pe6} [H(x - x_1) - H(x - x_2)] \left[H\left(y - y_1\right) - H\left(y - y_2\right) \right]. \tag{19}$$

The internal moments of the two-dimensional plate are specified by

$$M_x = -D_p \left(\frac{\partial^2 w}{\partial x^2} + v_p \frac{\partial^2 w}{\partial y^2} \right), \tag{20a}$$

$$M_y = -D_p\left(\frac{\partial^2 w}{\partial y^2} + v_p\frac{\partial^2 w}{\partial x^2}\right), \tag{20b}$$

$$M_{xy} = -(1-v_p)D_p\left(\frac{\partial^2 w}{\partial x\partial y}\right). \tag{20c}$$

The modified independent modal space control (MIMSC) method [20] is employed. That is, one piezoelectric actuator can control several modes at the same time. By assuming that the PZT patches do not significantly affect the dynamics of the plate, and using classical thin plate theory, the equation of motion can be described as

$$\frac{\partial^2(M_x - m_x)}{\partial x^2} + 2\frac{\partial^2(M_{xy} - m_{xy})}{\partial x\partial y} + \frac{\partial^2(M_y - m_y)}{\partial y^2} - C_s\dot{w} - \rho_p h_p\ddot{w} = 0. \tag{21}$$

Substituting Eqs. (16)–(20) into Eq. (21), the equation of motion is obtained as

$$\begin{aligned} D_p\nabla^4 w + C_s\dot{w} + \rho_p h\ddot{w} + \sum_{i=1}^{N_a}\Big\{ & C_0^i\varepsilon_{pe}^i[\delta'(x-x_{1i}) - \delta'(x-x_{2i})]\big[H(y-y_{1i}) - H(y-y_{2i})\big] \\ & + C_0^i\varepsilon_{pe}^i[H(x-x_{1i}) - H(x-x_{2i})]\big[\delta'(y-y_{1i}) - \delta'(y-y_{2i})\big] \\ & + 2C_0^i\,\varepsilon_{pe6}^i[\delta(x-x_{1i}) - \delta(x-x_{2i})]\big[\delta(y-y_{1i}) - \delta(y-y_{2i})\big]\Big\} = 0, \end{aligned} \tag{22}$$

where C_s is the structural damping operator, N_a is the number of the piezoelectric actuators, $\nabla^2 = \partial^2/\partial x^2 + 2(\partial^2/\partial x\partial y) + \partial^2/\partial y^2$, $\delta(x)$ is Dirac delta function, (x_{1i}, y_{1i}) and (x_{2i}, y_{2i}) are the down-left and top-right coordinate of the ith piezoelectric actuator, respectively.

The piezoelectric control equation of the plate can be written as the standard state-space form

$$\dot{z} = Az + B_p u_p, \tag{23}$$

$$y_{\text{current}} = C_p z, \tag{24}$$

where $z = [\eta_{11}\cdots\eta_{mn}\quad \dot{\eta}_{11}\cdots\dot{\eta}_{mn}]^{\mathrm{T}}$, $z \in R^{2(m\times n)\times 1}$ is the column vector composed of modal displacement and modal velocity; y_{current} is the current output of the piezoelectric sensor. Matrix A is

$$A = \begin{bmatrix} 0 & I \\ -\Omega^2 & -2\zeta\Omega \end{bmatrix}, \quad \big(A \in R^{2(m\times n)\times 2(m\times n)}\big), \quad \Omega = \mathrm{diag}(\omega_{ij}), \quad \zeta = \mathrm{diag}(\xi_{ij}),$$

where ω_{ij} and ξ_{ij} are the (i, j)th modal natural frequency and damping ratio, respectively. B_p and C_p are expressed as

$$B_p = M^{-1}\begin{bmatrix} B_{p1} \\ B_{p2} \end{bmatrix} = \begin{bmatrix} & & 0 & \cdots & 0 \\ & & \vdots & & \vdots \\ & & 0 & \cdots & 0 \\ M^{-1} & & \begin{bmatrix} \mathrm{piezo}_{11}^1 & \cdots & \mathrm{piezo}_{11}^{N_a} \\ \vdots & & \vdots \\ \mathrm{piezo}_{mn}^1 & \cdots & \mathrm{piezo}_{mn}^{N_a} \end{bmatrix} \end{bmatrix},$$

$$C_p = [C_{p1}\, C_{p2}] = \begin{bmatrix} \begin{matrix} 0 & \cdots & 0 \\ \vdots & & \vdots \\ 0 & \cdots & 0 \end{matrix} \\ \begin{bmatrix} \text{sensor}_{11}^{1} & \cdots & \text{sensor}_{11}^{N_s} \\ \vdots & & \vdots \\ \text{sensor}_{mn}^{1} & \cdots & \text{sensor}_{mn}^{N_s} \end{bmatrix} \end{bmatrix}^{\mathrm{T}},$$

where $B_p \in R^{2(m\times n)\times N_a}$, $(B_{p1}, B_{p2} \in R^{(m\times n)\times N_a})$ is the input matrix of the control value; $u_p = [V_1, \ldots, V_{N_a}]^{\mathrm{T}}$, $(u_p \in R^{N_a\times 1})$ is the control voltage of the actuator; $C_p \in R^{N_s\times 2(m\times n)}$ is the observed output matrix, $(C_{p1}, C_{p2} \in R^{N_s\times(m\times n)})$; N_s is the number of the piezoelectric sensors.

The coefficients of the piezoelectric actuator are given by

$$\begin{aligned} \text{Piezo}_{mn}^{i} = & -1/V_i \times \int_0^a \int_0^b \Big\{ C_0^i\, \varepsilon_{pe}^i \big[\delta'(x-x_{1i}) - \delta'(x-x_{2i})\big] \\ & \times \big[H\big(y-y_{1i}\big) - H\big(y-y_{2i}\big)\big] + C_0^i\, \varepsilon_{pe}^i [H(x-x_{1i}) - H(x-x_{2i})], \\ & \times \big[\delta'\big(y-y_{1i}\big) - \delta'\big(y-y_{2i}\big)\big] + 2C_0^i\, \varepsilon_{pe6}^i [\delta(x-x_{1i}) - \delta(x-x_{2i})] \\ & \times \big[\delta\big(y-y_{1i}\big) - \delta\big(y-y_{2i}\big)\big]\Big\} X_m(x)\, Y_n(y)\,\mathrm{d}x\,\mathrm{d}y, \end{aligned} \tag{25}$$

where $x = (x_{1i}+x_{2i})/2$, $y = (y_{1i}+y_{2i})/2$.

Farther derivation of Eq. (25) yields

$$\begin{aligned} \text{Piezo}_{mn}^{i} = & -1/V_i \times \Big\{ C_0^i\, \varepsilon_{pe}^i \big[X'_m(x_{2i}) - X'_m(x_{1i})\big] \int_{y_{1i}}^{y_{2i}} Y_n(y)\,\mathrm{d}y \\ & + C_0^i\, \varepsilon_{pe}^i \big[Y'_n\big(y_{2i}\big) - Y'_n\big(y_{1i}\big)\big] \int_{x_{1i}}^{x_{2i}} X_m(x)\,\mathrm{d}x \\ & + 2C_0^i\, \varepsilon_{pe6}^i [X_m(x_{2i}) - X_m(x_{1i})]\big[Y_n\big(y_{2i}\big) - Y_n\big(y_{1i}\big)\big]\Big\}. \end{aligned} \tag{26}$$

3. Optimal placement of the piezoelectric sensors and actuators

3.1. Placement performance indices

An optimal placement method of piezoelectric sensors and actuators for cantilever plate is given according to the maximum observability and controllability rule. Based on the sensors and actuators placement method presented by Gawronski [15], an optimal placement method by using H_2 norm is obtained, and the H_2 norm performance indices are derived for collocated sensors and actuators [21].

Let (A,B,C) be a state space representation of a linear system as given in Eqs. (23) and (24), the H_2 norm of the system is defined as [15]

$$\|G\|_2 = \sqrt{\left(\frac{1}{2\pi}\int_{-\infty}^{+\infty} tr(G^*(\omega)G(\omega))\mathrm{d}\omega\right)}, \tag{27}$$

where $G(\omega) = C_p(j\omega I - A)^{-1}B_p$, is the transfer function of the control system.

Considering the ith mode and its state space representation (A_i,B_i,C_i), the closed form expression can be obtained. Let $G_i(\omega) = C_i(j\omega I - A_i)^{-1}B_i$ be the transfer function of the ith mode. When the structural damping

ratio meets the condition $\xi_i \ll 1$, the H_2 norm of the ith mode can be expressed as

$$\|G_i\|_2 \cong \frac{\|B_i\|_2 \|C_i\|_2}{2\sqrt{\zeta_i \omega_i}}, \tag{28a}$$

where ω_i and ζ_i are the natural frequency and damping ratio of the ith mode, respectively.

When only the jth actuator has an input, the corresponding H_2 norm of the ith mode can be written as

$$\|G_{ij}\|_2 \cong \frac{\|B_{ij}\|_2 \|C_i\|_2}{2\sqrt{\zeta_i \omega_i}}. \tag{28b}$$

Because collocated placement of the sensors and actuators are adopted, the number of the sensors is equal to that of the actuators, that is, $N_a = N_s$. For the ith vibration mode, the modal H_2 norm of the jth input actuator to the jth output sensor is

$$\|G_{ijj}\|_2 \cong \frac{|B_{ij}||C_{ji}|}{2\sqrt{\zeta_i \omega_i}}, \tag{29}$$

where the matrices B_{ij} and C_{ji} are B_{p2} and C_{p2}, respectively.

By utilizing Eq. (29), the matrix norm is obtained. The optimal placement indices of the candidate locations of sensors and actuators are also obtained by means of the matrix two-norm.

The placement index δ_{2ij} that evaluates the input of the jth actuator to the output of the jth sensor for the ith mode is defined as

$$\delta_{2ij} = w_i^j \|G_{ijj}\|_2, \quad i = 1, \ldots, (m \times n), \quad j = 1, \ldots, N_s, \tag{30}$$

where $w_i^j \geqslant 0$ denotes the weight assigned to the jth actuator and the ith mode.

The weight w_i^j reflects the importance of the ith mode and the jth actuator in application, and the dimensions of the input (or output). In other words, it reflects the contribution of the controllability or observability. In general, the dominant mode weights are relatively larger than the others. In application, it is convenient to represent the two-norm placement indices as a placement matrix. The indices are

$$\Delta_2 = \begin{bmatrix} \delta_{2(11)1} & \cdots & \delta_{2(11)j} & \cdots & \delta_{2(11)N_S} \\ \cdots & \cdots & \cdots & \cdots & \cdots \\ \delta_{2i1} & \cdots & \delta_{2ij} & \cdots & \delta_{2iN_S} \\ \cdots & \cdots & \cdots & \cdots & \cdots \\ \delta_{2(mn)1} & \cdots & \delta_{2(mn)j} & \cdots & \delta_{2(mn)N_S} \end{bmatrix} \Leftarrow i\text{th mode}, \quad \Uparrow \quad j\text{th mode} \tag{31}$$

where the jth column consists of indices of the jth actuator for every mode, and the ith row is a set of the indices of the ith mode for all actuators.

Now, the H_2 norm optimal placement index for the jth actuator can be expressed as

$$\text{Max}: \quad \mu_{2aj} = \sqrt{\sum_{i=1\times 1}^{m\times n} \delta_{2ij}^2}, \tag{32a}$$

$$\text{Subject to}: \quad \frac{l_{pe}}{2} \leqslant x \leqslant a - \frac{l_{pe}}{2}, \quad \frac{k_{pe}}{2} \leqslant y \leqslant b - \frac{k_{pe}}{2}, \tag{32b}$$

where l_{pe} and k_{pe} are the length and the width of the piezoelectric patch, respectively; a and b are the length and the width of the plate, respectively.

The optimal index ensures the maximum placement index μ_{2aj} by selecting appropriate location of the jth actuator.

Remarks: when the orientation angle of the piezoelectric patches meets $\beta = 0$, only the bending modes can be measured and stimulated. When the orientation angle of the piezoelectric patches meets $\beta = \pi/4$, both the bending and torsional modes can be measured and stimulated by the piezoelectric patches. When pair patches stuck on both sides of the plate anti-symmetrically, in other words, on one side the orientation angle is $\beta = \pi/4$, and on the other side opposite to the same location orientation angle is $\beta = 3\pi/4$ stuck, thus, only the torsional modes can be measured and stimulated theoretically.

3.2. Simulation results and analysis

The simulation studies of optimal placement are carried out using the proposed method. The plate is a uniform aluminum plate with a rectangular cross section. The length, width and thickness of the rectangle plate are $a = 1.50\,\text{m}$, $b = 0.50\,\text{m}$ and $h = 1.50\,\text{mm}$, respectively. The material properties of the plate are as follows: Young's elastic modulus $E_p = 7.0 \times 10^{10}\,\text{N/m}^2$, Poisson's ratio $v_p = 0.33$ and density $\rho_p = 2700\,\text{kg/m}^3$. The structural damping ratio is 0.3%. The PZT patches are of $60\,\text{mm} \times 15\,\text{mm} \times 1\,\text{mm}$ in size. The parameters of the PZT patches are as follows: Young's elastic modulus $E_{pe} = 6.3 \times 10^{10}\,\text{N/m}^2$, Poisson's ratio $v_{pe} = 0.30$, density $\rho_{pe} = 7650\,\text{kg/m}^3$, piezoelectric strain constant is $d_{31} = d_{32} = 166 \times 10^{-12}\,\text{m/V}$, $d_{36} = 0\,\text{m/V}$.

The nodal line of torsional modes is in the center of the chordwise direction. In order to obtain the torsional moment for controlling the torsional modes, the piezoelectric sensors and actuators should be placed along nodal line. For bending modes, the piezoelectric actuators can be placed evenly along the chordwise direction. Then, the optimal locations of PZT patches are considered only in the spanwise direction.

Theoretically, the flexible plate is an infinite-dimensional system, however, the number of excited modes is finite due to finite energy. Here, we retain only the first five modes. The retaining modes include three bending modes and two torsional modes. The natural frequencies of bending modes are $\omega_{11} = 0.57\,\text{Hz}$, $\omega_{21} = 3.59\,\text{Hz}$, $\omega_{31} = 10.06\,\text{Hz}$; and those of torsional modes are $\omega_{12} = 3.81\,\text{Hz}$, $\omega_{22} = 12.10\,\text{Hz}$. The weights of bending modes are 50, 10 and 1, respectively; and those of torsional modes are 25 and 5, respectively.

By using Eq. (32a), the optimal placement results for bending and torsional modes are shown in Figs. 2 and 3, respectively. From Fig. 2, one knows that for suppressing bending modal vibration, the piezoelectric sensors and actuators should be located at the root of the plate, with orientation angle $\beta = 0^\circ$. From Fig. 3, one knows that for suppressing torsional vibration, sensors and actuators should be located at the tip of the plate, with orientation angle $\beta = 45^\circ$, as shown in Fig. 1. The collocated placement of sensors and actuators is adopted.

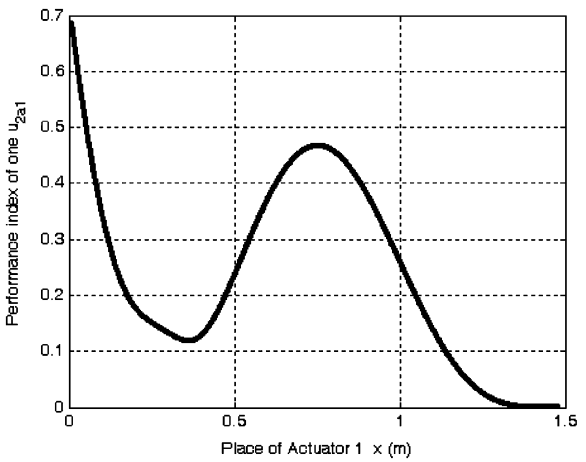

Fig. 2. Performance index μ_{2a1} for bending modes.

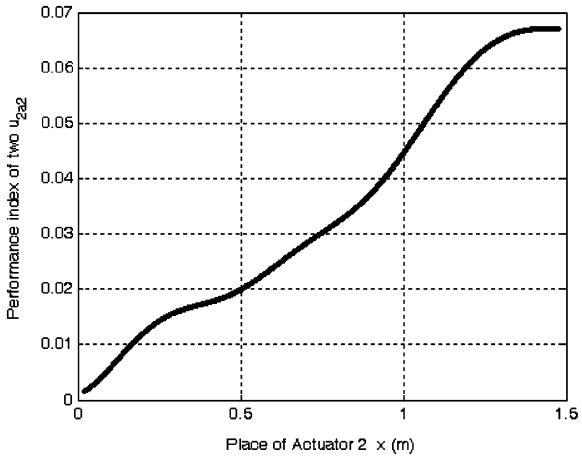

Fig. 3. Performance index μ_{2a2} for torsional modes.

4. Control methods and simulation results

4.1. PPF and the controller by combining PPF and PD

PPF control method is used to suppress the vibration of large flexible structures presented by Fanson and Caughey [12] and Goh and Caughey [23]. PPF controller has several distinguished advantages as compared with the widely used velocity feedback control laws. It is insensitive to spillover that contributions from unmodeled modes affect the control of the modes of interest [12,22]. As a second-order low-pass filter, a PPF controller rolls off quickly at high frequencies. Thus, the approach is well suited to controlling the lower modes of a structure with well-separated modes, as the controller is insensitive to the unmodeled high frequency dynamics. In addition, PPF controller is easy to implement. Because of these advantages, PPF controller along with smart materials, in particular PZT type of piezoelectric material has been applied to many flexible systems to achieve active damping.

PPF controller requires that the sensor is collocated or nearly collocated with the actuator. In PPF controller, structural position information is fed to a compensator. The output of the compensator, magnified by a gain, is fed directly back to the structure. The equations describing PPF operation are given as [12,22]

$$\text{Structure}: \quad \ddot{\xi} + 2\zeta\omega\dot{\xi} + \omega^2\xi = u, \quad u = k\omega^2\eta, \tag{33}$$

$$\text{Compensator}: \quad \ddot{\eta} + 2\zeta_c\omega_c\dot{\eta} + \omega_c^2\eta = \omega_c^2\xi, \tag{34}$$

where ξ is a modal coordinate describing displacement of the structure, ζ and ω are the damping ratio and natural frequency of the structure, respectively; k is feedback gain, η is the compensator coordinate, ζ_c and ω_c are the damping ratio and natural frequency of the compensator, respectively; u is the control input to the system.

The PPF controller can be expressed as the following transfer function form by Laplace transform

$$\frac{u}{\xi} = \frac{k\omega^2\omega_c^2}{s^2 + 2\zeta_c\omega_c s + \omega_c^2}. \tag{35}$$

The natural frequency required in the design of PPF controller cannot be known exactly, or may vary with time. When the frequencies used in the PPF controller are different from those of the structure, the performance of the PPF control will adversely affected. So ω_c should be equal or closed to ω, hence, the natural vibration characteristics should be known a priori either theoretically or experimentally in order to successfully apply the PPF controller. This process is called the tuning process. Because the closed-loop system

should be stable, the control gain should satisfy

$$0<k<1. \tag{36}$$

From Eq. (36) one can know that PPF control method has the localization of having a small control gain, which must be below 1, and this small gain will weaken the performance of vibration suppression of flexible structures. To overcome this problem, a control method by combining PPF and PD is proposed to improve the performance of PPF controller, and the excellent results can be gained. The combining PPF and PD control algorithm is given as

$$u = k\omega^2\eta - K_p\xi - K_v\dot{\xi}, \tag{37}$$

where $K_p>0$ and $K_v>0$ are proportional and derivative gains of PD controller, respectively.

According to Routh's stability theory, when $\omega\approx\omega_c$, and to ensure the stability of the closed-loop system, the control gain should satisfy

$$0<k<1+\frac{K_p}{\omega^2}. \tag{38}$$

Comparing Eq. (38) with Eq. (36), one can know that the control method by combining PPF and PD can increase the range of feedback gain k, under the same condition that the stability of the system is guaranteed.

The decay rate of PPF control algorithm is

$$\zeta_b\omega_b = \left(\zeta+\frac{k\beta}{2\alpha}\right)\omega. \tag{39}$$

The decay rate of the control method by combining PPF and PD is

$$\zeta_b\omega_b = \left(\zeta+\frac{k\beta}{2\alpha}+\frac{K_v}{2\omega}\right)\omega\sqrt{1+\frac{K_p}{\omega^2}}. \tag{40}$$

Comparing Eq. (40) with Eq. (39), it can be seen that the control method by combining PPF and PD can increase the decay rate of the system comparing to PPF method without decreasing the stability, so the suppression of vibration can be gained dramatically.

4.2. Simulation results

Distributed structures are infinite-dimensional. Since it is impossible, in practice, to control or estimate the entire infinity of modes, vibration control of such a structure is limited to a finite number of modes by the modal truncation [24]. In this paper, only the first three vibration modes are targeted as the control modes, including the first two bending modes and the first torsional mode. The rectangle thin plate is made of fiberglass colophony. The length of the cantilever plate is 1.5 m, and its width and thickness are 0.5 m and 1.78 mm, respectively. The material properties of plate such as Young's modulus, Poisson's ratio and mass density are $E_b = 34.64$ Gpa, $v_b = 0.33$ and $\rho_b = 1840\,\mathrm{kg/m^3}$, respectively. Using Eq. (12), one can obtain that the natural frequencies of the first two bending modes are $\omega_{11} = 0.59$ Hz, $\omega_{21} = 3.47$ Hz. The natural frequency of the first torsional mode is $\omega_{12} = 3.71$ Hz. The parameters of PZT patches are given in Section 3.2. We assume that the nominal value of damping ratio is 0.006 for all the first three modes.

The purpose of simulation is to show that the proposed control algorithms can dissipate energy from targeted modes, and the convergence and effectiveness of the optimal placement for the sensors and actuators. The simulation results of the first bending mode are shown in Fig. 4. Fig. 4(a) shows the free vibration of the first bending mode without control. Fig. 4(b) shows the calculated result of PD control, in which the control gains of PD method are $K_p = 0.5$ and $K_d = 0.15$. Fig. 4(c) shows the simulation result of PPF control, in which the parameters of PPF controller are $\zeta_{c1} = 0.707$, $\omega_{c1} = 0.57$ and $k_1 = 0.98$, respectively. Fig. 4(d) shows the result by the control method by combining PPF and PD. From the simulation results of the first bending mode vibration control, one can know that the bending vibration is suppressed effectively by the adopted control methods, and the proposed method shows perfect stability and convergence.

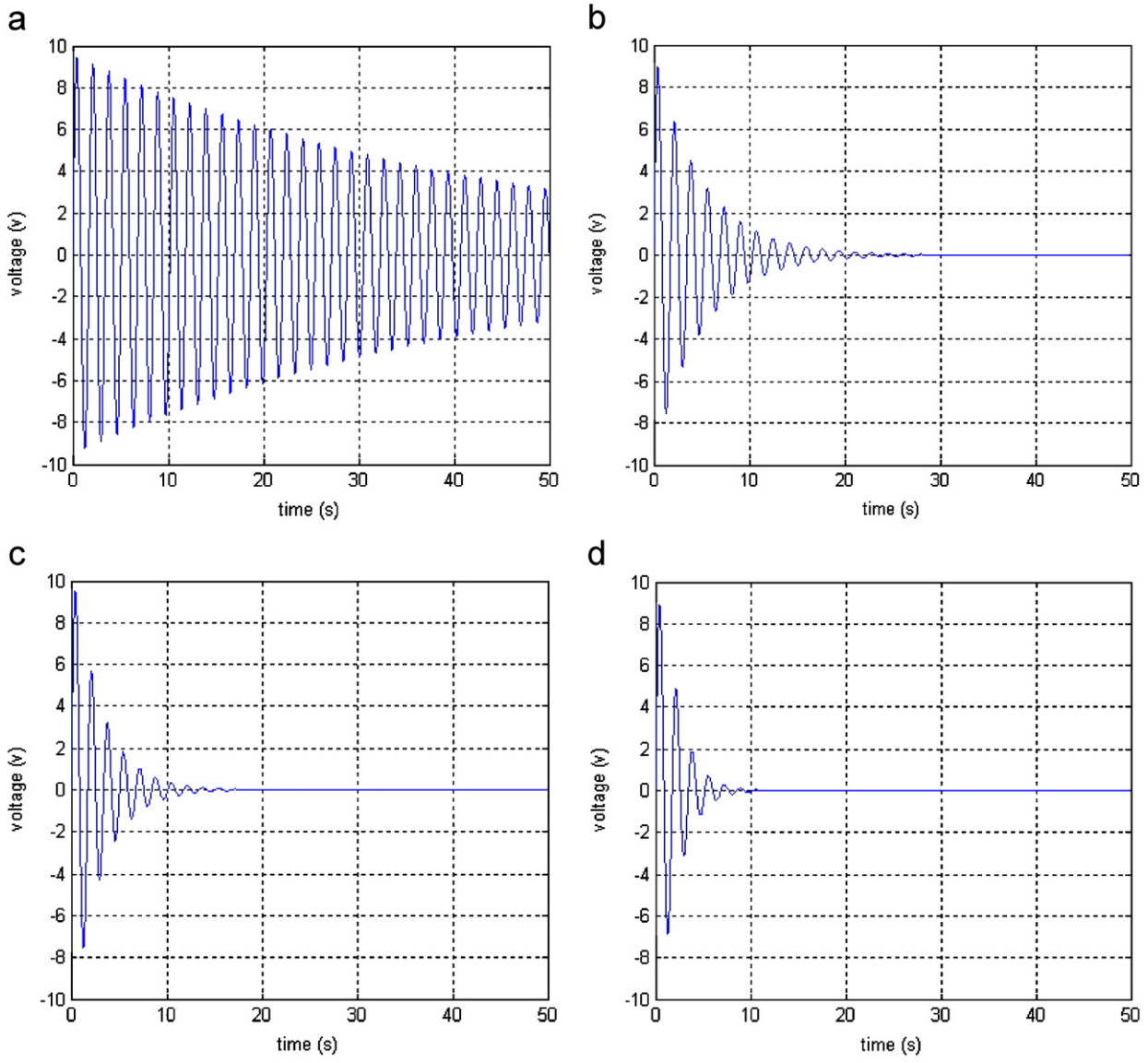

Fig. 4. The numerical results of the first bending mode: (a) without control; (b) PD control method; (c) PPF control method; and (d) the control method by combining PPF and PD.

The simulation results of suppressing the first two bending modes vibration are shown in Fig. 5, where the controller parameters are selected as those of the previous studies of the first bending mode. From the simulation results, one can know that the proposed control method still shows good stability and convergence even for the multi-mode control.

The simulation results of the first bending mode are shown in Fig. 6. Fig. 6(a) shows the free vibration of the first torsional mode without control. Fig. 6(b) shows the calculated result of PD control, in which the gains of PD controller are $K_p = 0.25$ and $K_d = 0.06$. Fig. 6(c) shows the simulation result of PPF control, in which the parameters of PPF controller are $\zeta_{c3} = 0.707$, $\omega_{c3} = 3.75$ and $k_3 = 0.98$. Fig. 6(d) shows the numerical result of the control method by combining PPF and PD. From the simulation results of the first torsional vibration mode, it can be seen that the proposed control method can suppress the torsional vibration effectively.

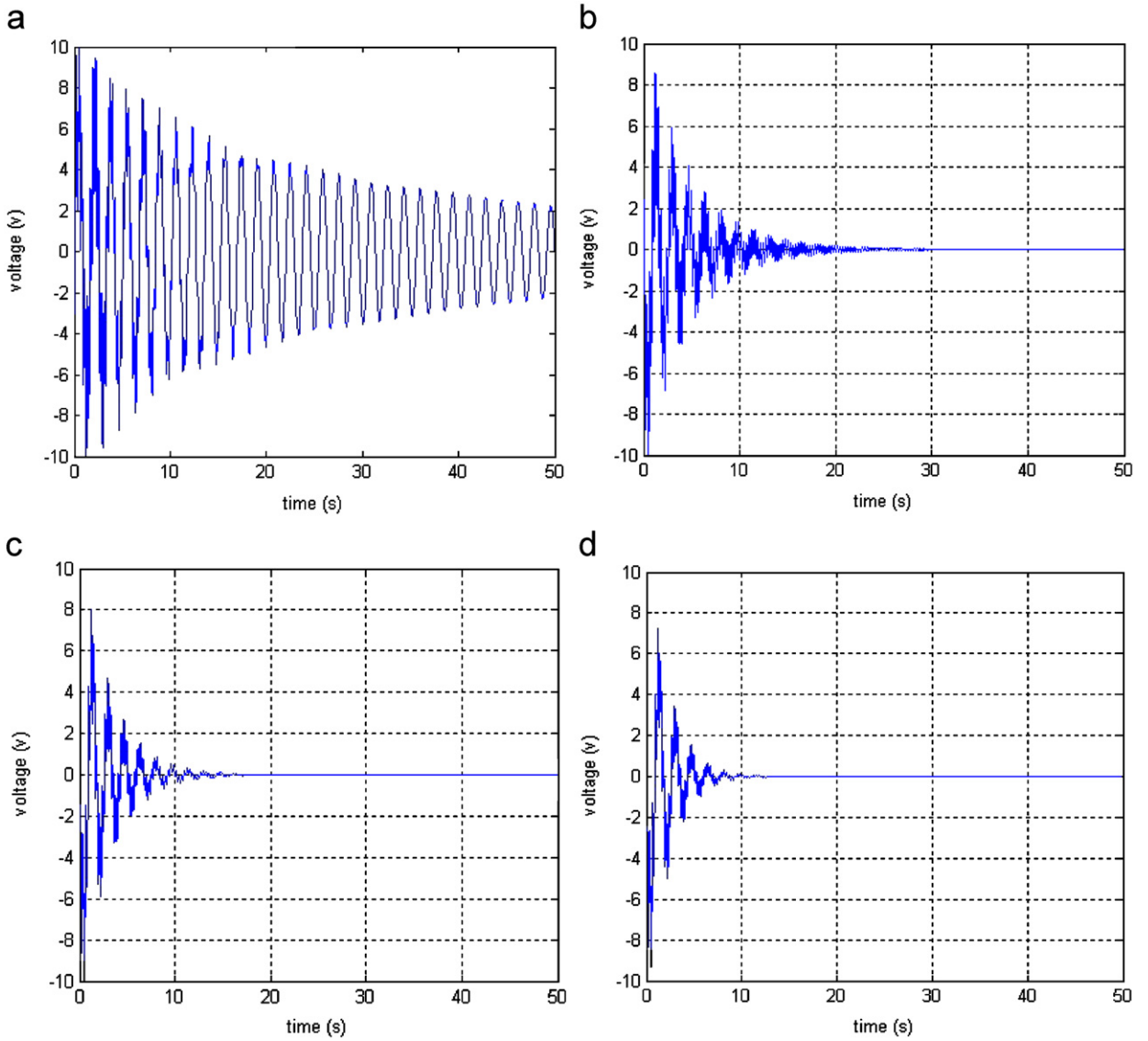

Fig. 5. The numerical results of the first two bending modes: (a) without control; (b) PD control method; (c) PPF control method; and (d) the control method by combining PPF and PD.

The piezoelectric sensors and actuators used in the simulation studies are located according to the optimal placement results in Section 4, and the simulation results show that the placement is effective, and the vibration can be suppressed quickly.

5. Experimental results

5.1. The experimental test-bed

The sketch map of the piezoelectric patch placed in the plate is shown in Fig. 7. The plate is made of fiberglass colophony. The size and material parameters of the cantilever plate are given in Section 4.2. The parameters of the discrete distributed surface-mounted PZT patches are given in Section 3.2. The piezoelectric sensors and actuators are bonded to the host structure using strong epoxy adhesive material.

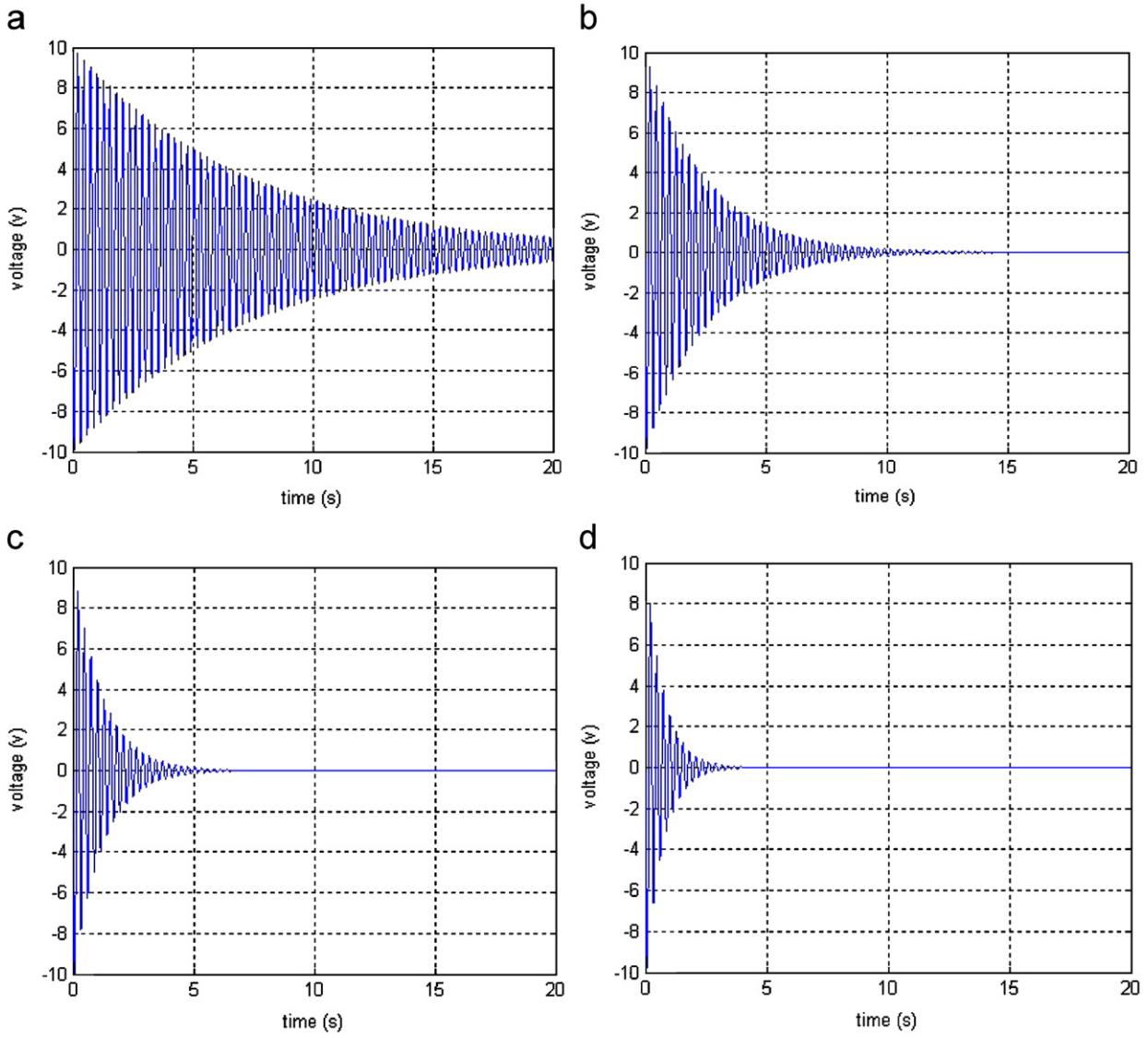

Fig. 6. The numerical results of the first torsional mode: (a) without control; (b) PD control method; (c) PPF control method; and (d) control method by combining PPF and PD.

The photograph of the cantilever plate setup is shown in Fig. 8. The piezoceramic patches are bonded symmetrically for bending modes and anti-symmetrically for torsional modes to each side of the plate. In total, five sensed and control circuits are considered, and the serial number is from one to five. Serial number one is the circuit at the clamped end, the fifth is the channel at the tip, and the rest can be deduced by analogy. Only two circuits are used in the experiments, they are the first circuit and the fifth circuit for the bending and the torsional modal vibration suppression, respectively. Thus, the sensors and actuators used to control the bending and torsional vibration modes are approximately collocated.

Charger amplifiers YE5850 can amplify the signals measured by strain sensor. Power amplifier amplifies the output control voltages to a suitable value. An industrial personal computer (IPC) is used for the data acquisition and system control. The signals are converted from analog-to-digital and digital-to-analog through a 16-channel 12-bit A/D board and 12-channel 12-bit D/A board, respectively. The sampling period of the controller is 1ms.

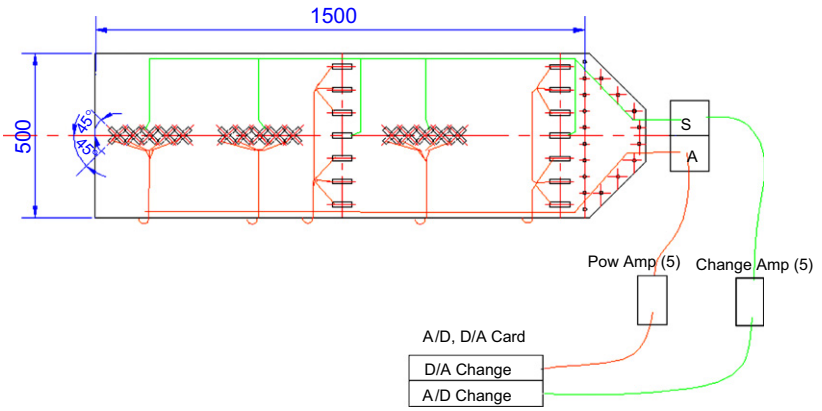

Fig. 7. The sketch map of the piezoelectric patch placed in the plate.

Fig. 8. Photograph of the experimental setup.

5.2. Experimental validation of the optimal placement of sensors and actuators

The high-frequency modes can be neglected on physical grounds, because such modes only play a secondary role in determining the model's essential characteristics and the energy concentrates on the low-frequency modes primarily, thus, the high-frequency modes are truncated in the experimental system. In the experimental studies, the first two bending modes and the first torsional mode are mainly considered in these results.

In order to validate the optimal placement of sensors and actuators, stimulation analysis was carried out for an actual plate, as shown in Fig. 8. After stimulation, the time-domain responses of the fourth channel and the fifth channel are measured at the same time shown in Fig. 9. Because the orientation angle of the fourth and the fifth channel sensors are 45°, both the bending and the torsional modes can be simultaneously measured. After fast Fourier transform (FFT) of the time-domain responses shown in Fig. 9, the frequency responses are shown in Fig. 10. Comparing Fig. 10(a) with Fig. 10(b), it can be seen that the magnitudes of the bending modes measured by the fourth channel are larger than those of the fifth channel. On the contrary, the magnitude of the torsional mode measured by the fourth channel is less than that of the fifth channel. In other words, the PZT patches located near to the root of the plate are helpful to measure and control the bending modes; and those near to the tip end are beneficial to torsional mode. Therefore, the optimal placement carried out in the previous section is proved.

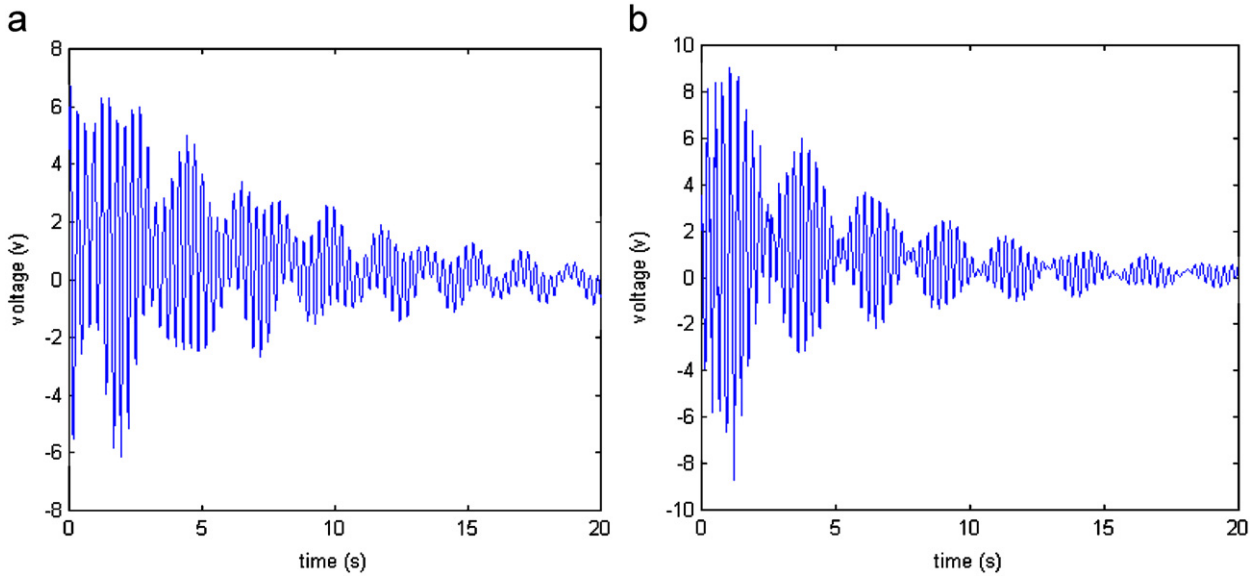

Fig. 9. Time-domain responses of the fourth and the fifth channel signals: (a) the fourth channel signal; and (b) the fifth channel signal.

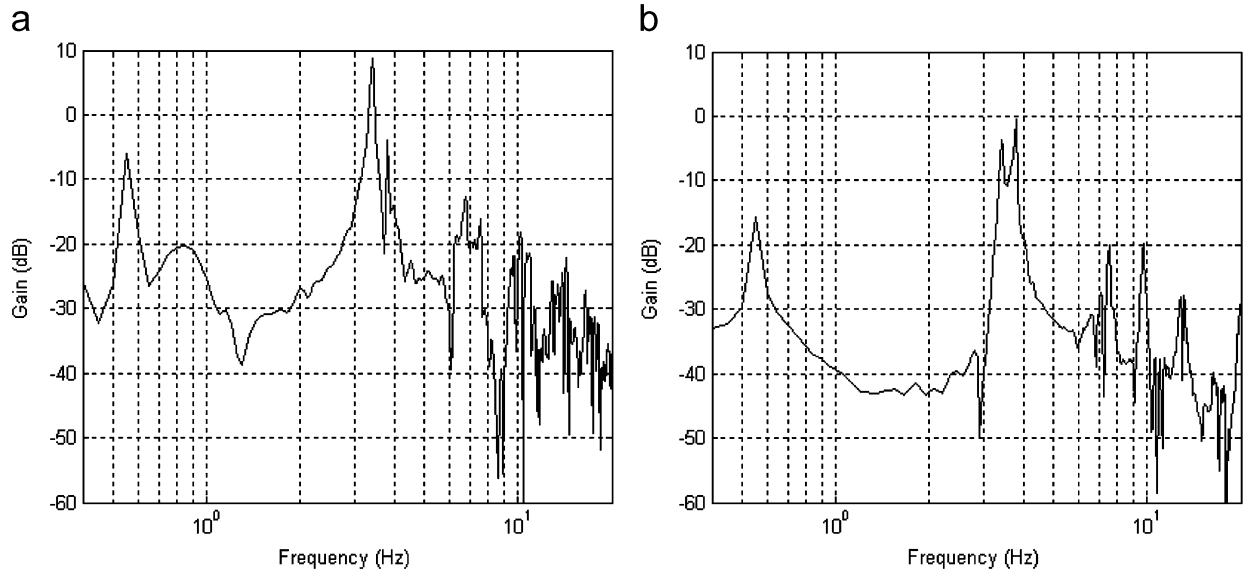

Fig. 10. Frequency responses of the fourth and the fifth channel signals after FFT: (a) FFT of the fourth channel's measurement; and (b) FFT of the fifth channel's measurement.

In the vibration control of the flexible plate structure, the presence of uncontrolled or unmodeled modes within the bandwidth of the closed-loop system results in the well-known phenomenon of "spillover". Figs. 9 and 10 show that the bending modes and torsional mode are coupled. Here, decoupling for bending and torsional modes of the cantilever plate in measurement and control is realized by combining with Butterworth band-pass filter as shown in Fig. 11. Besides, multiple PZT patches are used at the same time and the average effect are introduced, so the observe spillover and control spillover can be prevented. Although the placement of sensors and actuators is transversely non-collocated, we can make sure that the system is still a minimum

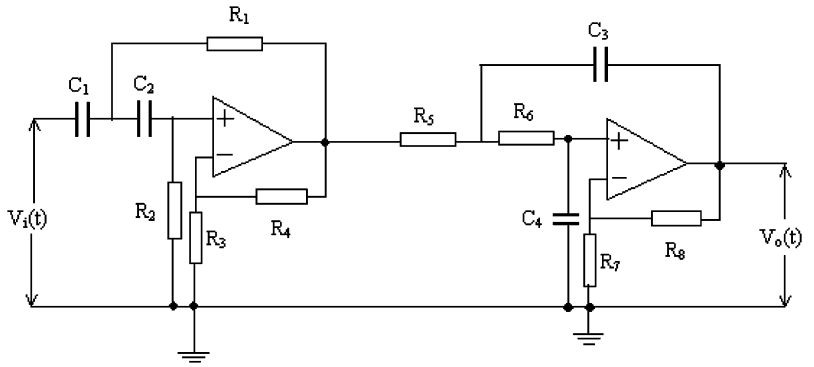

Fig. 11. The analog band-pass Butterworth filter.

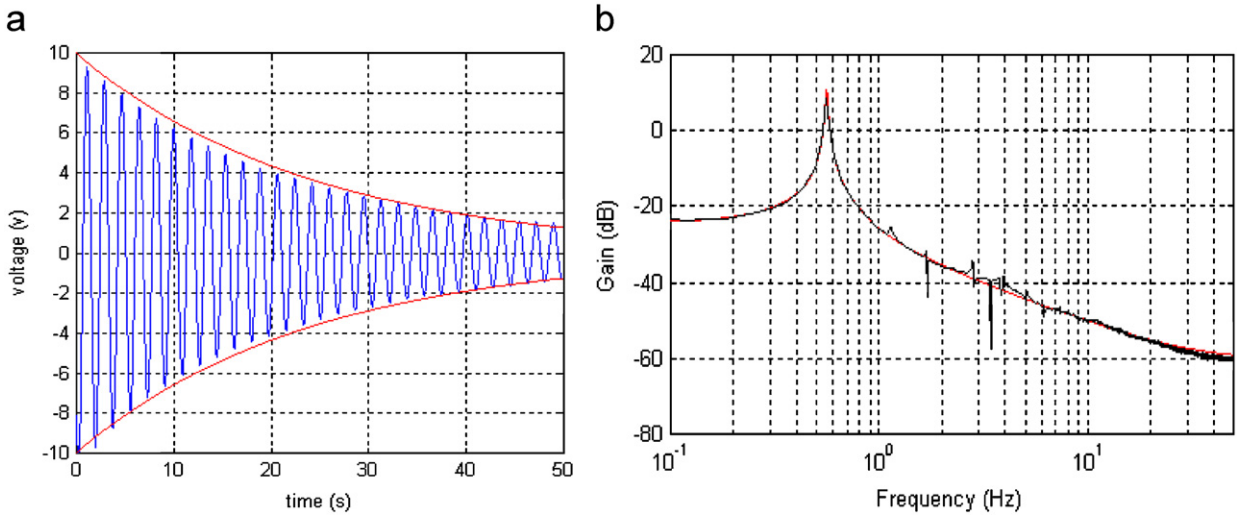

Fig. 12. The measured responses of the first bending mode without control: (a) time-domain response; and (b) frequency response.

phased system, which resolves not only the local control problem caused by collocated placement, but also the non-minimum phased problem due to lengthwise non-collocated placement. Thus, the optimal placement of sensors and actuators can be adopted for vibration control of the cantilever plate. The next sections include modal identification and implementation of control methods.

5.3. *Experimental identification on modal frequencies and damping ratio of the system*

After stimulation, the time-domain response and its curve envelope of the first bending mode without control are depicted in Fig. 12(a), and one can obtain the frequency response shown in Fig. 12(b) by FFT. The curve fitting of the frequency response can be expressed as the following transfer function approximately

$$G(s) = \frac{9.410 \times 10^{-4}(s + 4.001)(s + 199.505)}{(s + 0.0415 - 3.518\mathrm{i})(s + 0.0415 + 3.518\mathrm{i})}. \tag{41}$$

From Eq. (41) it can be derived that the zeros are $z_1 = -199.45$, $z_2 = -4.001$, the poles $p_{1,2} = -0.0415 \pm 3.518\mathrm{i}$, the gain $k = 9.410 \times 10^{-4}$. The damping ratio and modal frequency of the first bending mode are $\zeta_1 = 0.0118$ and $\omega_1 = 0.56\,\mathrm{Hz}$, respectively.

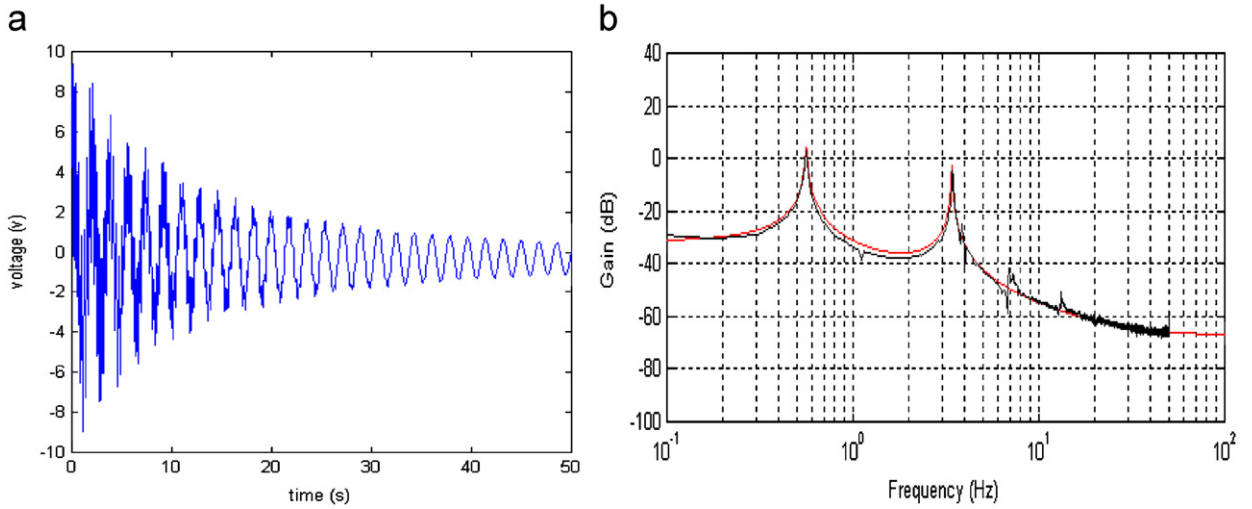

Fig. 13. The responses of the first two bending modes without control: (a) time-domain response; and (b) frequency response.

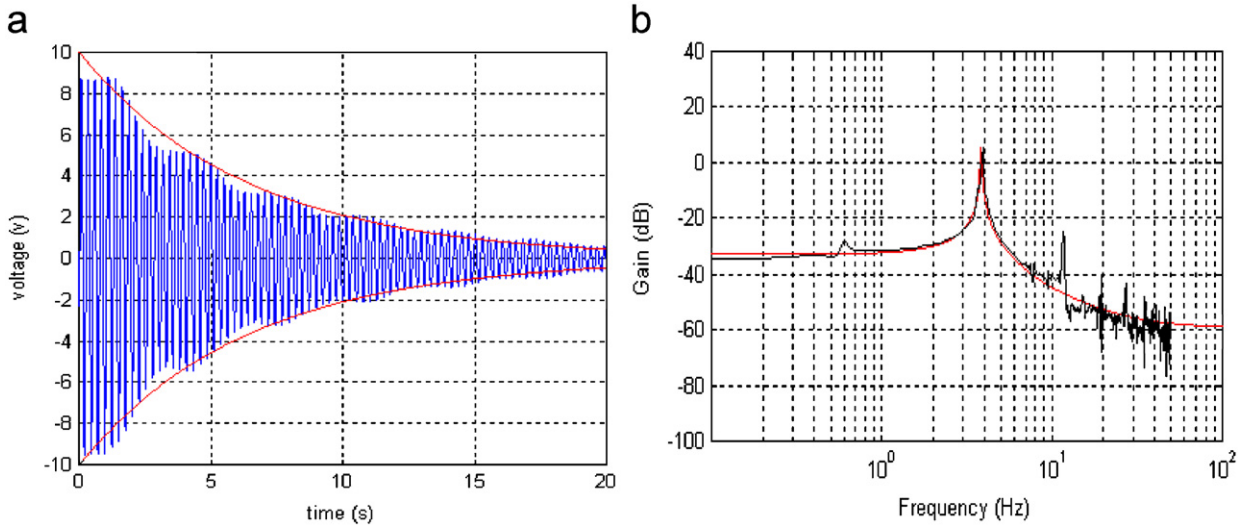

Fig. 14. The free vibration responses of the first torsional mode: (a) time-domain response; and (b) frequency response.

The time-domain response of the first two bending modes without control is depicted in Fig. 13(a), and the frequency response shown in Fig. 13(b) can be obtained by FFT. The curve fitting of the frequency response can be expressed as

$$G(s) = \frac{4.277 \times 10^{-4}(s+4.001)(s+199.505)(s+30.0)(s+15.0)}{(s+0.0415 \pm 3.518\mathrm{i})(s+0.126 \pm 21.362\mathrm{i})}. \tag{42}$$

From Eq. (42) one can know that the zeros are $z_1 = -199.45$, $z_2 = -30.00$, $z_3 = -15.00$ and $z_4 = -4.001$; the poles are $p_{1,2} = -0.0415 \pm 3.518\mathrm{i}$ and $p_{3,4} = -0.126 \pm 21.362\mathrm{i}$; the gain of the system is $k_1 = 4.277 \times 10^{-4}$, the damping ratio and modal frequency of the first bending mode are $\zeta_1 = 0.0118$ and $\omega_1 = 0.56\,\mathrm{Hz}$, those of the second bending mode are $\zeta_2 = 0.0059$ and $\omega_2 = 3.40\,\mathrm{Hz}$, respectively.

The damping ratio of the first bending mode is larger than that of analytical study due to the air damping effect. And the practical frequencies of the plate system are approximately equal to the analytical results, the difference is mainly due to the effect of the bonded PZT and the material property is not uniform.

The time response and curve envelope of the torsional mode without control is shown in Fig. 14(a), and the frequency response shown in Fig. 14(b) can be obtained by FFT. The curve fitting of the frequency response can be expressed as

$$G(s) = \frac{1.075 \times 10^{-3}(s + 58.365)(s + 203.731)}{(s + 0.156 - 24.001\mathrm{i})(s + 0.156 + 24.001\mathrm{i})}. \tag{43}$$

From Eq. (43) one obtains the zeros $z_5 = -203.731$ and $z_6 = -58.365$; the poles $p_{5,\,6} = -0.156 \pm 24.001\mathrm{i}$, the gain is $k_2 = 1.075 \times 10^{-3}$; the damping ratio and modal frequency of the first torsional mode are $\zeta_3 = 0.0065$ and $\omega_3 = 3.82\,\mathrm{Hz}$, respectively.

The identified modal frequencies are approximately equal to those of the analytical results. The differences are mainly dependent on the effect of the bonding PZT patches and the parameter uncertainties. After identification, the modal frequencies and damping ratios of the open-loop system for the cantilever plate are obtained. And the modal frequencies are used to design PPF controller.

From Eqs. (42) and (43), it can be known that the zeros of the plate system are far away from the imaginary axis, so the poles of the first three modes dominate the system. The pole map of the first three modes is shown in Fig. 15. From Fig. 15, one can know that the poles of the first three modes locate in the left half complex plane, thus the system is stable. When the control algorithms are applied to the plate system, the closed-loop system is stable if the real parts of the eigenvalue are negative, and the system is convergent.

5.4. Experimental study on active vibration control of the system

The time-domain closed-loop responses of the first bending mode are shown in Fig. 16, and those of the first two bending modes are shown in Fig. 17. Figs. 16(a) and 17(a) show the closed-loop responses by using PD control method. Figs. 16(b) and 17(b) show those of PPF control method, and Figs. 16(c) and 17(c) show those of the control method by combining PPF and PD.

Comparing Figs. 16 and 17 with Figs. 9 and 10, respectively, it can be seen that the bending modes vibration can be suppressed quickly. The proposed control method by combining PPF and PD can damp out the vibration effectively. The vibration was suppressed approximately in 10 s.

The time-domain closed-loop responses of the torsional mode vibration control are shown in Fig. 18. Fig. 18(a), (b) and (c) show the experimental results by using PD controller, PPF controller and the combining PPF and PD controller, respectively. From these results one can know that PD control method can suppress

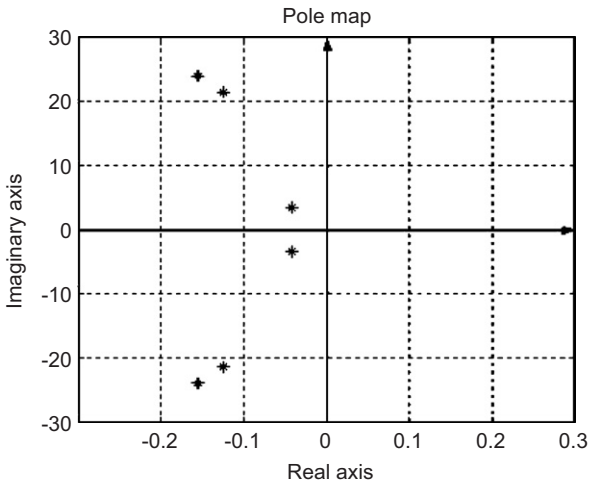

Fig. 15. The poles of the cantilever plate for the first three modes without control.

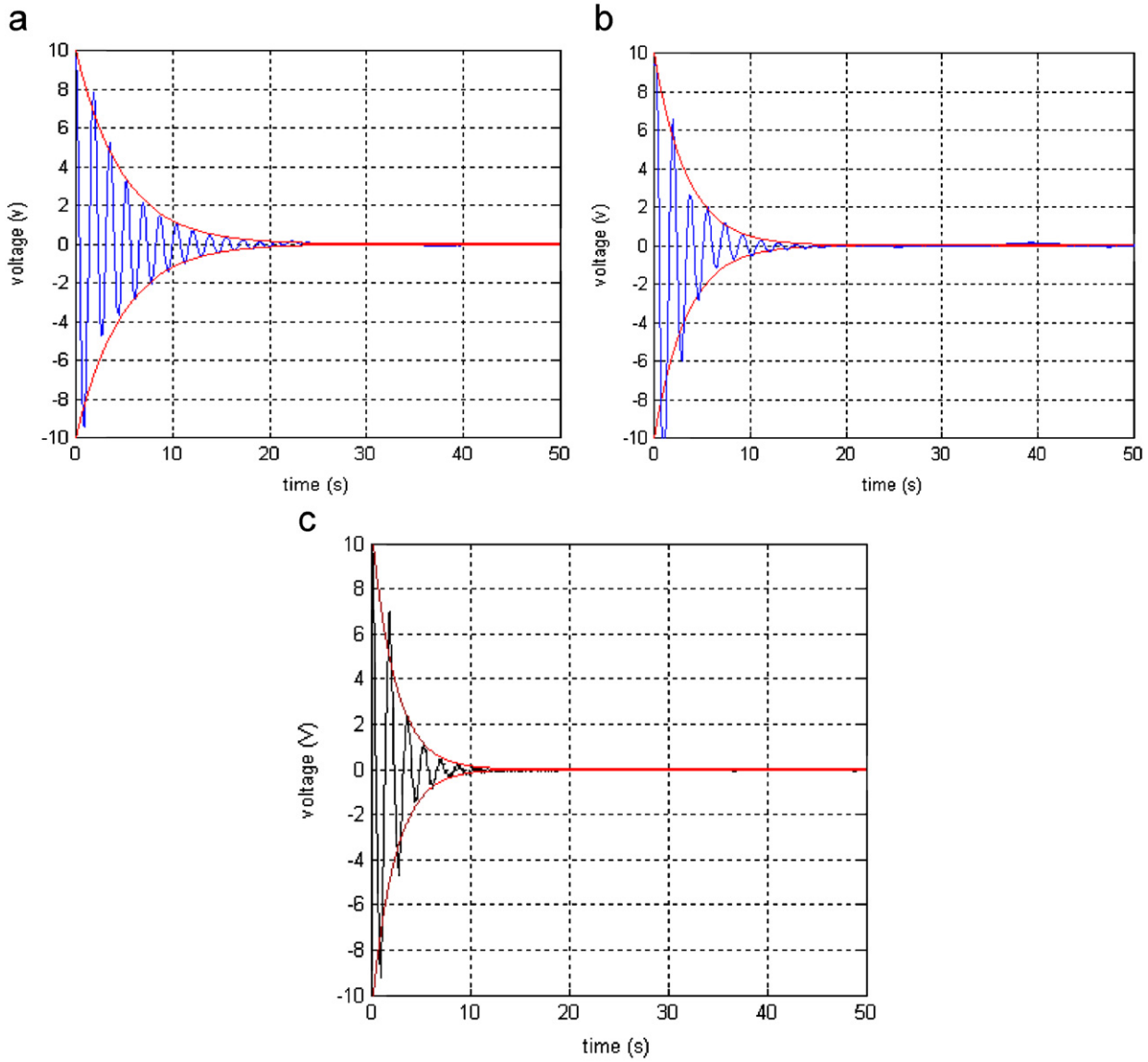

Fig. 16. The controlled time-domain responses of the first bending mode: (a) PD control method; (b) PPF control method; and (c) the control method by combining PPF and PD.

the larger vibration amplitude significantly, but vibration of the smaller amplitude will last for a period of time. PPF control method can suppress the smaller vibration amplitude significantly. The proposed control method combining PPF and PD can reduce both the larger and the smaller vibration amplitudes effectively.

Comparing all the experimental results with those of the simulation results, it can be seen that they are approximately same. The existent differences mainly due to the following reasons: (a) the nonlinear behavior of the actuators and sensors, such as saturation, dead zone, hysteretic nonlinearity; (b) process disturbance, the inaccuracy of sensors and measured noise; and (c) the parameters of the host material and PZT can not be accurately known, etc. The experimental results show that the optimal placement is feasible, and the proposed control method can suppress the vibration effectively and shows good stability and convergence.

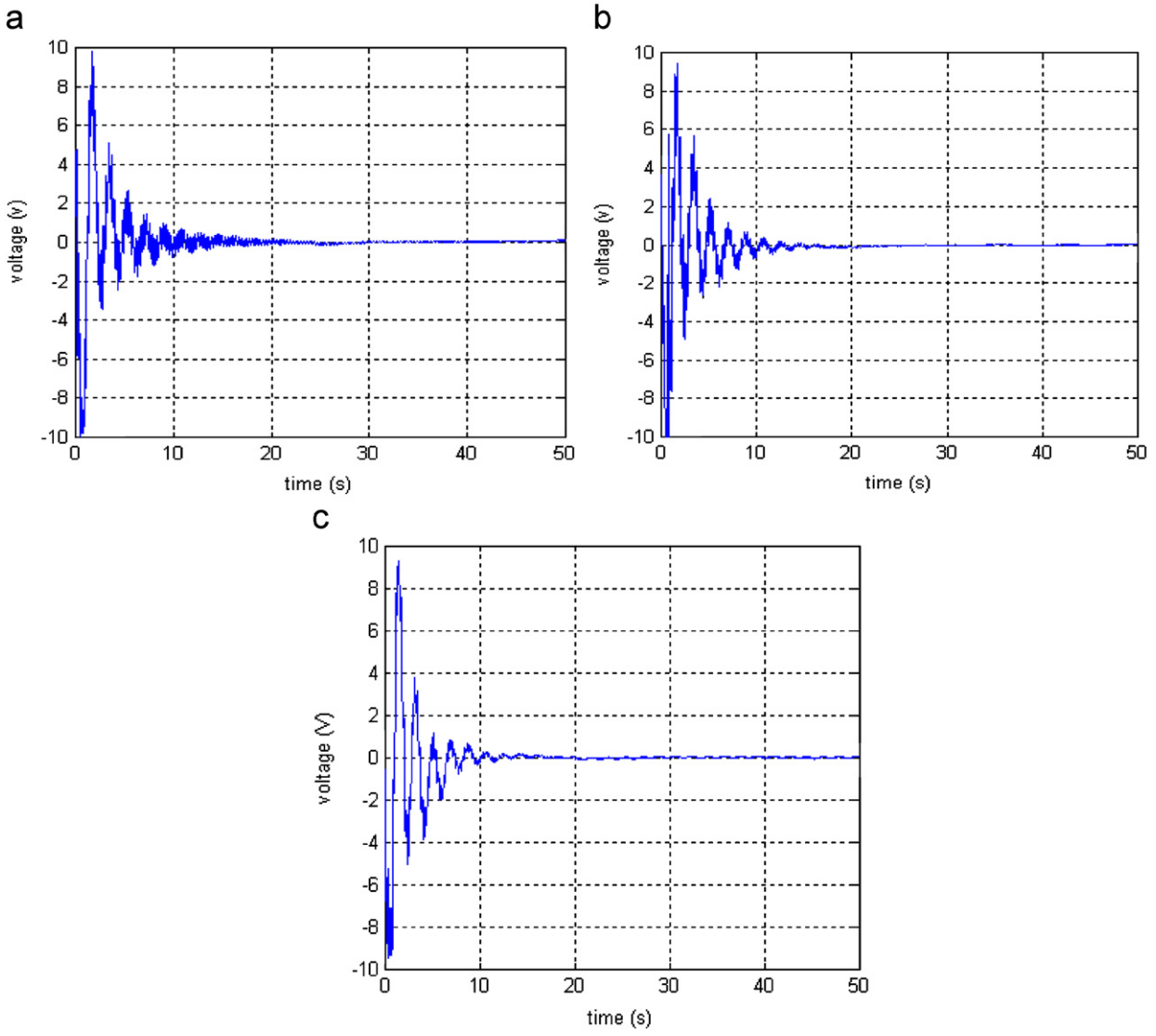

Fig. 17. The controlled time-domain responses of the first two bending modes: (a) PD control method; (b) PPF control method; and (c) the control method by combining PPF and PD.

6. Conclusions

This paper presents the theoretical analysis and experimental results of vibration suppression of a flexible cantilever plate bonded with PZT sensors and actuators. From the theoretical studies and experimental results we can know that the presented method of optimal placement for the cantilever plate is feasible. By using two-order Butterworth band-pass filter and average effect of multiple piezoelectric ceramics, the decoupling of the bending and torsional modes is realized, and the spillover problem can be prevented in the closed-loop bandwidth. Simulations and experimental results on the actual process have shown that the proposed control method by combining PPF and PD can suppress the vibration effectively, especially for vibration decay process and the smaller amplitude vibration.

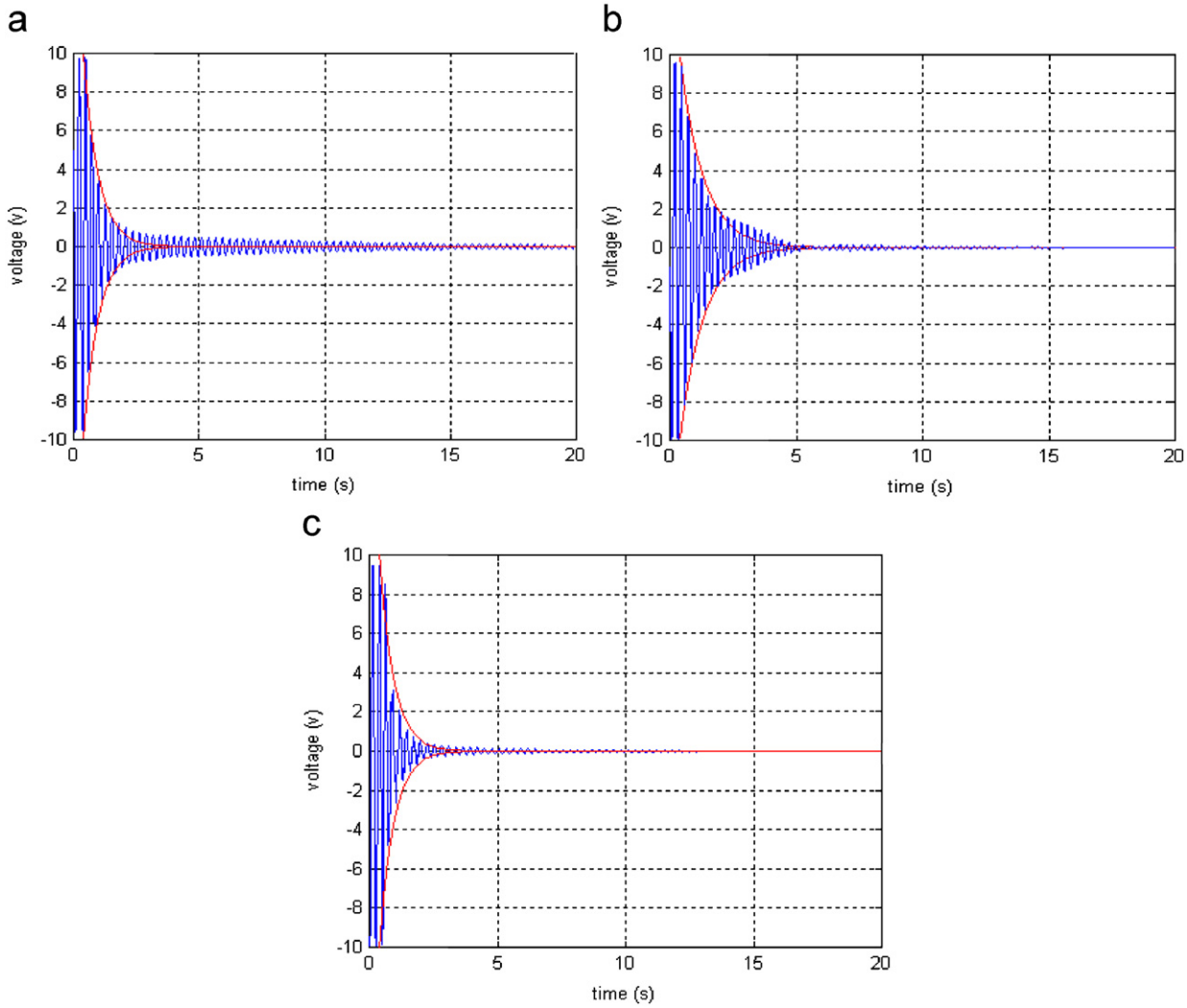

Fig. 18. Experimental results for active control of torsional mode by different methods: (a) PD control method; (b) PPF control method; (c) the control method by combining PPF and PD.

Acknowledgements

This research was supported by the National Natural Science Foundation of China under grants 60404020, 90505014 and 60034010; the authors gratefully acknowledge their support. In addition, the authors would like to thank the anonymous Reviewers for their constructive comments.

References

[1] D.C. Hyland, J.L. Junkins, R.W. Longman, Active control technology for large space structures, *Journal of Guidance Control and Dynamics* 16 (1993) 801–821.

[2] D.C. Sun, L.Y. Tong, D.J. Wang, Vibration control of plate using discretely distributed piezoelectric quasi modal actuators and sensors, *AIAA Journal* 39 (2001) 1766–1772.

[3] T. Bailey, J.E. Hubbard, Distributed piezoelectric-polymer active vibration control of a cantilever beam, *Journal of Guidance Control and Dynamics* 8 (1985) 605–611.

[4] E. Crawley, J. de Luis, Use of piezoelectric actuators as elements of intelligent structures, *AIAA Journal* 25 (1987) 1373–1385.
[5] E. Crawley, K.B. Lazarus, Induced strain actuation of isotropic and anisotropic plates, *AIAA Journal* 29 (1991) 944–951.
[6] H.S. Tzou, H.Q. Fu, A study of segmentation of distributed piezoelectric sensors and actuators. Part I: Theoretical analysis, *Journal of Sound and Vibration* 172 (1994) 247–272.
[7] C.R. Fuller, S.J. Elliott, P.A. Nelson, *Active Control of Vibration*, Academic Press, San Diego, CA92101, 1996.
[8] R.L. Clark, W.R. Saunders, G. Gibbs, *Adaptive Structures Dynamics and Control*, Wiley, Inc., 1998.
[9] L. Meirovitch, *Dynamics and Control of Structures*, Wiley, New York, 1990.
[10] L. Gaudiller, S. Bochard, Adaptive active control of flexible structures subjected to rigid body displacements, *Journal of Sound and Vibration* 283 (2005) 311–339.
[11] C.K. Lee, F.C. Moon, Modal sensors/actuators, *Journal of Applied Mechanics* 57 (1990) 434–441.
[12] J.L. Fanson, T.K. Caughey, Positive position feedback control for large space structures, *AIAA Journal* 28 (1990) 717–724.
[13] P. Shimon, E. Richer, Y. Hurmuzlu, Theoretical and experimental study of efficient control of vibrations in a clamped square plate, *Journal of Sound and Vibration* 282 (2005) 453–473.
[14] Y. Li, J. Onoda, K. Minesugi, Simultaneous optimization of piezoelectric actuator placement and feedback for vibration suppression, *IAA ACTA Astronautic Journal* 50 (2002) 335–341.
[15] W.K. Gawronski, *Dynamics and Control of Structures: A Modal Approach*, Springer, New York, Inc., 1998.
[16] V.S. Rao, S. Sana, An overview of control design methods for smart structural system, *SPIE* 4326 (2001) 1–13.
[17] P. Liu, V.S. Rao, M. Derriso, Active control of smart structures with optimal actuator and sensor locations, *SPIE* 4693 (2002) 1–12.
[18] M.L. Deorenzo, Sensor and actuator selection for large space structure control, *Journal of Guidance Control and Dynamics* 13 (1990) 249–257.
[19] J.A. Rule, R.E. Richard, R.L. Clark, Design of an aero elastic delta wing model for active flutter control, *Journal of Guidance Control and Dynamics* 24 (2001) 918–924.
[20] A. Baz, S. Poh, Experimental implementation of the modified independent modal space control method, *Journal of Sound and Vibration* 139 (1990) 133–149.
[21] Z. Qiu, Optimal placement of sensors and actuators for flexible plate of vibration suppression, *Journal of Astronautics* 23 (2002) 30–36 (in Chinese).
[22] G. Song, S.P. Schmidt, B.N. Agrawal, Experimental robustness study of positive position feedback control for active vibration suppression, *Journal of Guidance* 25 (2002) 179–182.
[23] C.J. Goh, T.K. Caughey, On the stability problem caused by finite actuator dynamics in the collocated control of large space structures, *International Journal of Control* 41 (1985) 787–802.
[24] C. Mei, B.R. Mace, Reduction of control spillover in active vibration control of distributed structures using multi-optimal schemes, *Journal of Sound and Vibration* 251 (2002) 184–192.
[25] L. Cheng, Q. Tang, D. Li, The characteristics of nonlinear vibration of extending structure of space vehicle, *Aerospace Shanghai* 18 (2001) 1–3 (in Chinese).